J Mater Sci (2026) 61:19853–19865

Metals & corrosion

Development and thermo-mechanical characterization of NiMnTi melt-spun ribbons

Francesca Villa[1,2,*], Emanuele Bestetti[1], Mariana Rios[3], Lara Righi[4], Fabio Lazzari[1], Francesca Passaretti[1], Volodymyr Chernenko[3,5,6], Daniel Salazar[3], Riccardo Casati[2], and Elena Villa[1]

[1] *Institute of Condensed Matter Chemistry and Technologies for Energy (CNR ICMATE), National Research Council, Via G. Previati 1/E, 23900 Lecco, Italy*
[2] *Department of Mechanical Engineering, Politecnico Di Milano, Via Privata G. La Masa 1, 20156 Milano, Italy*
[3] *BCMaterials, Basque Center for Materials, Applications and Nanostructures, EHU Science Park, 48940 Leioa, Spain*
[4] *Dipartimento Di Scienze Chimiche, Università Di Parma, Della Vita E Della Sostenibilità Ambientale, Parco Area Delle Scienze 17/A, 43124 Parma, Italy*
[5] *University of the Basque Country (UPV/EHU), 48080 Bilbao, Spain*
[6] *Basque Foundation for Science, 48009 Bilbao, Spain*

Received: 3 March 2026
Accepted: 16 May 2026
Published online:
28 May 2026

ABSTRACT

All-d-metal Heusler alloys, particularly NiMnTi-based alloys, have gained increasing attention due to their superior mechanical and caloric properties compared to traditional NiMn-based systems. These alloys exhibit robust metallic bonding, which enhances ductility and superelasticity, making them promising candidates for functional applications. Melt spinning is an effective method for producing polycrystalline NiMn-based thin ribbons; however, there remains a research gap concerning the functional and thermo-mechanical characterization of the benchmark NiMnTi alloy. The present study investigates the effects of the melt spinning process on the microstructural, structural, calorimetric, functional and mechanical properties of two NiMnTi alloys with Ti contents of 15 at.% and 18 at.%. The results suggest that wheel speed may play a relevant role in the development of residual stresses, thickness inhomogeneity and solidification defects in NiMnTi ribbons, thereby influencing their calorimetric, mechanical and functional properties. The potential elastocaloric response of NiMnTi ribbons is preliminarily investigated, highlighting the necessity of further improvements and optimization for potential future developments in mini- and microscale elastocaloric devices.

Handling Editor: Jae-il Jang.

Address correspondence to E-mail: francesca.villa@cnr.it

E-mail Addresses: emanuelebestetti@cnr.it; mariana.rios@bcmaterials.net; lara.righi@unipr.it; fabio.lazzari@cnr.it; francesca.passaretti@cnr.it; volodymyr.chernenko@ehu.eus; daniel.salazar@bcmaterials.net; riccardo.casati@polimi.it; elena.villa@cnr.it

https://doi.org/10.1007/s10853-026-13013-2

Introduction

All-d-metal alloys are an emerging class of Heusler alloys that exhibit improved mechanical properties with respect to the traditional NiMn-based systems, including NiMnTi-based alloys [1, 2]. Indeed, in NiMn-based alloys, the strong covalent interaction between the constitutive elements caused by the *p–d* orbital hybridization promotes an intrinsic brittleness [2]. Conversely, since *all-d-metal* alloys are exclusively composed of elements from the *3d* transition group, they are characterized by a *d–d* orbital hybridization in which the valence electrons are uniformly distributed and therefore generate a strong metallic bonding [2]. This allows remarkable mechanical properties that are beneficial to the potential application of these alloys.

Among *all-d-metal* alloys, NiMnTi-based alloys are gaining increasing research interest for their exceptional mechanical, functional and caloric properties. In particular, superelasticity up to 7% and elongation at break up to 13% are achieved by these systems [2–4]. Some studies investigate the elastocaloric effect of NiMnTi and NiMnTi-based alloys that is associated with the high entropy change and volume change of the unit cell involved in the thermoelastic martensitic transformation [5–10]. The highest elastocaloric performance has been found in directionally solidified textured samples with adiabatic ΔT up to 37.3 °C and ΔS up to 50 J/(kg °C) [10]. By the addition of Co [11], it is possible to enhance the magnetic properties and therefore the magnetocaloric behavior of NiMnTi alloys. For instance, the partial substitution of Ni with Co has been shown to enhance the ferromagnetic interaction between Co and Mn atoms in the parent phase, leading to a more pronounced thermally driven magnetization change coupled with the structural transition [12–15]. Similarly, the substitution of Ni with Zn has been shown by Bachagha et al. [16] to shift both the martensitic transformation (MT) and Curie temperatures to lower values.

NiMnTi and related alloys are typically produced by means of casting methods, i.e., traditional arc melting [7, 17, 18], directional solidification processes [2, 10, 19, 20], and single crystal growth [21]. Only a few studies have reported the production of NiMnTi-based alloys by melt spinning, and these have primarily focused on alloys with Co addition for magnetic and magneto-functional applications [22–26]. Melt spinning allows the production of polycrystalline alloys with fine, textured microstructures and homogeneous composition. It has proven to be an effective method for synthesizing traditional Heusler alloys such as NiMnGa, NiMnSn, NiMnIn, NiFeGa, and their derivatives [27–31]. This technique involves the rapid solidification of a molten alloy onto a water-cooled rotating wheel with a polished surface typically made of copper. By melt spinning, it is possible to cool down the material from the liquid phase with cooling rates in the order of 10^4–10^6 K/s [32]. Such rapid quenching enables the formation of alloys with unique microstructures, including metastable phases and refined grains [33, 34]. For instance, rapid solidification in melt-spun NiMn-Sn/In ribbons favors the formation of the lower-symmetry B2 cubic structure, by suppressing the formation of higher-symmetry $L2_1$ [22, 32, 33]. In contrast, in other studies, a single $L2_1$ austenite phase was obtained [30, 31, 34–36]. The crystalline structure of melt-spun ribbons often exhibits columnar grains in the cross section, extending from the bottom to the top surface, perpendicular to the ribbon plane [32, 35]. Another characteristic of melt-spun ribbons is their preferential crystallographic orientation, which results in pronounced texturing [32, 34, 35, 37]. It has been found for NiMn-Sn/In that melt spinning process promotes grain refinement [33–37], leading to a decrease of the martensitic transformation temperatures [33]. For instance, martensitic transformation temperatures of NiMnSn ribbons are about 150K lower than those of conventionally cast ingots [32].

The few studies about NiMnTiCo melt-spun ribbons investigate mainly the magnetocaloric properties of the material. The most interesting results are reported by Neves-Bez et al. showing magnetic entropy change of 27 J/(kg °C) and cycling mechanical stability [25]. Ni-rich and Mn-rich ribbons in both as-spun [24, 38] and annealed conditions [22, 23, 25, 26] have been thoroughly investigated from the calorimetric, microstructural, structural and magnetic point of view. It was found that an increase in Co content and a refinement of the microstructure lead to a decrease in the transformation temperatures [22]. Moreover, it is proven that the process parameters, in particular the wheel speed, also affect the physical, functional and magnetic properties of the ribbons. Ma et al. [24] showed that by increasing the wheel speed the structural parameters, i.e., average grain size and unit cell volume, are decreased together with the martensitic transformation temperatures and the magnetic entropy change. NiMnTiCo alloys modified with B and Y have been shown to be able to enhance the magnetocaloric properties [38, 39]. Finally, the development of NiMnTiCo ribbons/polymer composites toward possible applications in magnetic devices with a flexible substrate has been investigated in ref. [40].

The present work aims to investigate the effect of melt spinning and heat treatment parameters on the physical, microstructural, calorimetric, functional and mechanical properties of two NiMnTi-based alloys, i.e., $Ni_{50}Mn_{35}Ti_{15}$ and $Ni_{50}Mn_{32}Ti_{18}$ (atomic %). The study explores the effects of the process parameters on the ribbons' properties to understand how the manufacturing process influences the material's structure, martensitic transformation and performance. Several characterization techniques—such as X-ray diffraction (XRD), scanning electron microscopy (SEM), differential scanning calorimetry (DSC), as well as mechanical and functional testing—are employed to investigate the alloy's behavior and to preliminarily assess its potential for elastocaloric applications. This study aims to fill the gap regarding the production of the benchmark NiMnTi alloy through melt spinning to define a roadmap toward a possible miniaturization of functional devices.

Materials and methods

Two series of NiMnTi ingots were produced by means of an arc melting furnace starting from high purity metallic elements (electrolytic Ni with purity level of 99.97%, electrolytic Mn with purity level of 99.5% and grade 1 Ti wire ASTM B348) and following six remeltings. Their compositions are $Ni_{50}Mn_{35}Ti_{15}$ and $Ni_{50}Mn_{32}Ti_{18}$ (at.%), and they were labeled NMT15 and NMT18 respectively.

An *Edmund Bühler Melt-Spinner SC* was employed to produce the NiMnTi ribbons. The arc-melted ingots were cut into 9–11g pieces to ensure uniform heating inside the induction-heated crucible. Quartz crucibles were manually prepared by softening and shaping the edges of quartz tubes with a diameter of 10 mm and a wall thickness of 1 mm. All crucibles were fabricated with circular nozzles having diameters ranging from 0.80 to 0.85 mm. The distance between the nozzle and the copper wheel was fixed at 1.5 mm. An ejection pressure of 700 mbar was chosen in order to avoid excessive Mn evaporation during the induction melting step, with a pressure difference of 200 mbar used to eject the molten alloy onto the copper wheel. The linear wheel speed (WS) was tuned between 10 and 40 m/s. The as-spun samples were labeled according to their alloy composition and the wheel speed used during the production process: NMT15_10 / 15 / 20 / 30 / 35 / 40 and NMT18_10 / 15 / 20 / 25 / 30 / 35 / 40. The microstructural, morphological and compositional characteristics of the ribbons were assessed through SEM and energy-dispersive X-ray analysis (EDX). Calorimetric analysis was performed by means of DSC *TA Instruments* Q200 with a heating and cooling rate of 10 °C/min. The transformation temperatures were determined at the intersection of the tangent lines drawn at the inflection points of the peaks and at the baseline. The X-ray diffraction (XRD) analysis was carried out on entire ribbon samples by means of an X-ray Diffractometer *Panalytical XPert PRO* equipped with a thermal chamber for measurements below and above room temperature, for the study of the martensitic and parent phases. The mechanical characterization of the ribbons consisted of both strain recovery and stress–strain tests in tensile configuration by means of a dynamic thermal and mechanical analyzer (DMTA *TA Instruments* Q800) equipped with a load cell of 18 N. The strain recovery tests were performed with a rate of 5 °C/min at fixed applied stresses (from 0.5 to 100 MPa) between 40 and 250 °C for NMT15 alloy and between-180 and 130 °C for NMT18 alloy. The stress–strain measurements were carried out with a stress rate of 5 MPa/min up to stresses between 150 and 250 MPa. Quasi-adiabatic tensile and bending measurements were carried out with an applied force rate equal to 150 N/min. The temperature signal was acquired by means of *T*-type thermocouples with bare wires of a diameter equal to 0.127 mm fixed on the sample surface with silver paste and connected to a high-frequency acquisition system (NI 9212 thermocouple input module for NI CompactDAQ) controlled by *National Instruments* LabView software.

Results and discussion

A detailed microstructural, calorimetric, functional, mechanical and caloric characterization of the precursor NiMnTi arc-melted alloy was carried out in previous works [17, 18].

Ribbons morphology analysis

The transversal cross sections of NiMnTi melt-spun ribbons were analyzed by means of scanning electron microscopy. The thickness of the ribbons is inhomogeneous, and the average values decrease with increasing wheel speed (WS). Particularly, the reduction in thickness between the lowest WS (10 m/s) and 25 m/s is approximately 50% for both alloys. At higher WS, the thickness tends to stabilize around a limit value of approximately 25 µm. Figure 1 summarizes the thickness trend measured for NMT15 and NMT18.

Moreover, SEM micrographs of the fractured cross sections of the melt-spun ribbons are shown in the insets in Fig. 1a and b for NMT15 and NMT18, respectively. The fracture occurs principally with intergranular mode. Particularly in the ribbons produced at the lowest WS, the characteristic microstructure of melt-spun ribbons is visible, featuring equiaxial grains in correspondence of the "wheel side" of the ribbon, which was subjected to the highest cooling rate, and columnar grains extending along the heat extraction direction in the cross section. For both alloys, grain size decreases with increasing WS, as higher cooling rates limit the grain growth.

Martensitic transformation

The wheel speed parameter significantly affects the martensitic transformation behavior of the as-spun ribbons. Both NMT15 and NMT18 produced with wheel speeds up to 30 m/s show sharp transformation DSC peaks, as shown in Fig. 2. In contrast, ribbons produced at higher speeds (35 and 40 m/s) exhibit lower and broader peaks, likely indicating that the material does not transform homogeneously. As a possible consequence, the complete transformation occurs over a wider temperature range. As will be further discussed in the XRD section and as observed in different previous works [27, 28], the extremely rapid solidification promoted by melt spinning process is consistent with the formation of solidification defects distributed in the textured grain structure of the obtained ribbons. This could have a first consequence in the wide transformation temperature range observed in DSC curves and in XRD patterns. Moreover, the peculiar inverse strain recovery and functional behavior presented in the following section will provide further suggestion about the fact that the solidification defects could act as stress-pinning points, likely introducing transformation inhomogeneity and residual stresses stored in the material.

A structural characterization of NiMnTi melt-spun ribbons was carried out through XRD analysis at different temperatures, i.e., above and below the martensitic transformation temperature range. Figure 3 presents the results obtained for samples produced at 20 m/s.

In both samples, a typical Heusler face-centered cubic (FCC) austenitic structure was observed at high temperatures, whereas a monoclinic martensitic phase was identified at low temperatures through Lebail fitting. Preferential orientation of grains is indicated by the pronounced intensity of the peaks corresponding

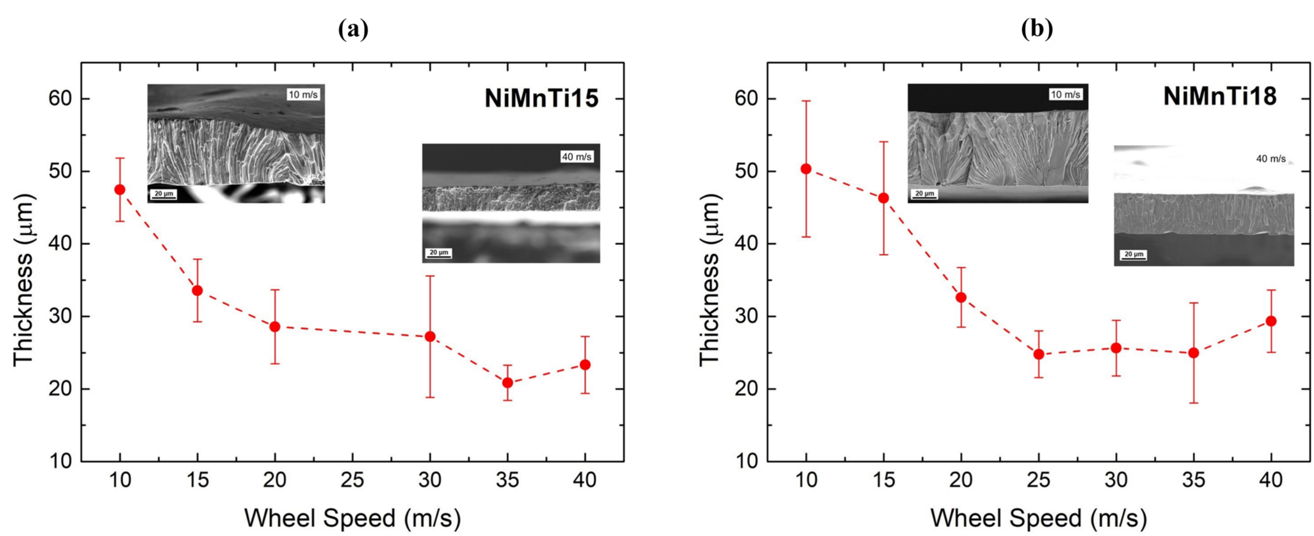

Figure 1 Trend of the NMT15 **a** and NMT18 **b** melt-spun ribbons thickness (measured from cross-section SEM micrographs in the inset) at increasing wheel speed.

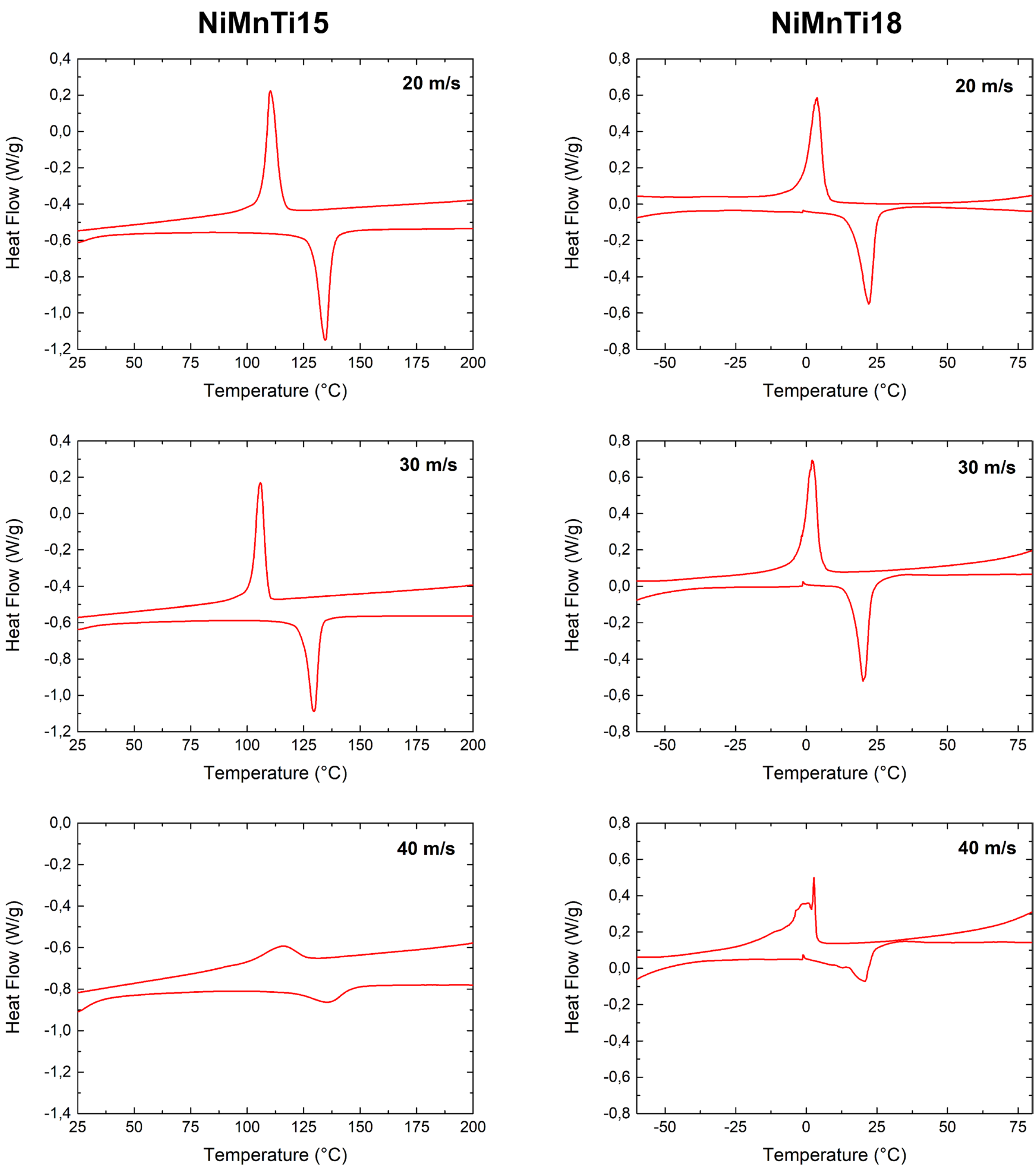

Figure 2 Differential scanning calorimetry of NMT15 and NMT18 ribbons produced with a wheel speed of 20 m/s, 30 m/s, and 40 m/s. Exothermal direction: up.

to the (121) reflection of the monoclinic cell. The XRD patterns of samples produced at wheel speeds ranging from 10 m/s to 30 m/s exhibited an almost exact correspondence in terms of crystal lattice parameters for both alloys. Figure 4 presents a comparison of the martensitic phases in ribbons produced at low (10 m/s)

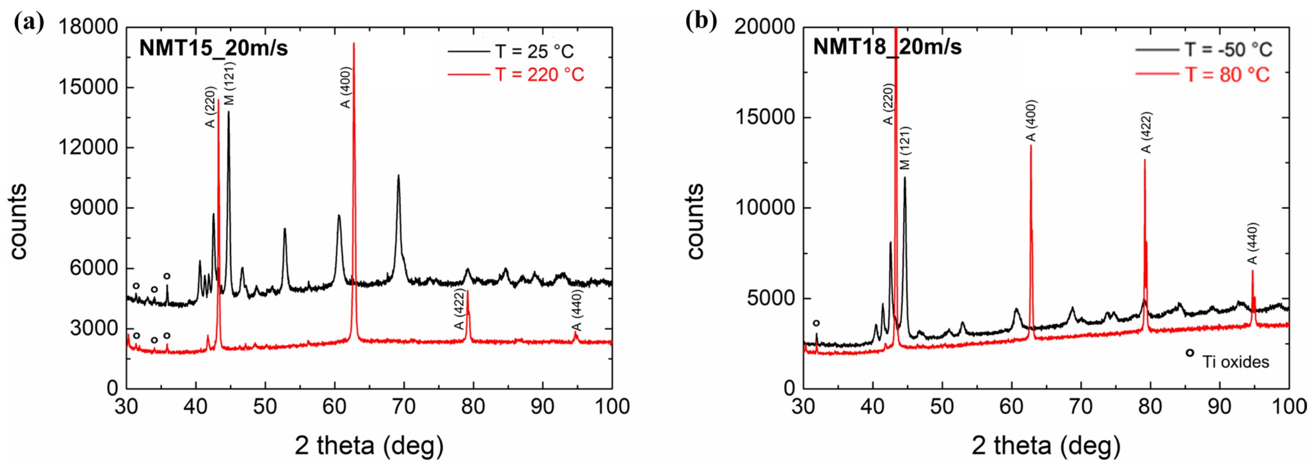

Figure 3 X-ray diffraction analysis below and above the martensitic transformation temperature range for ribbons NMT15_20 **a** and NMT18_20 **b**.

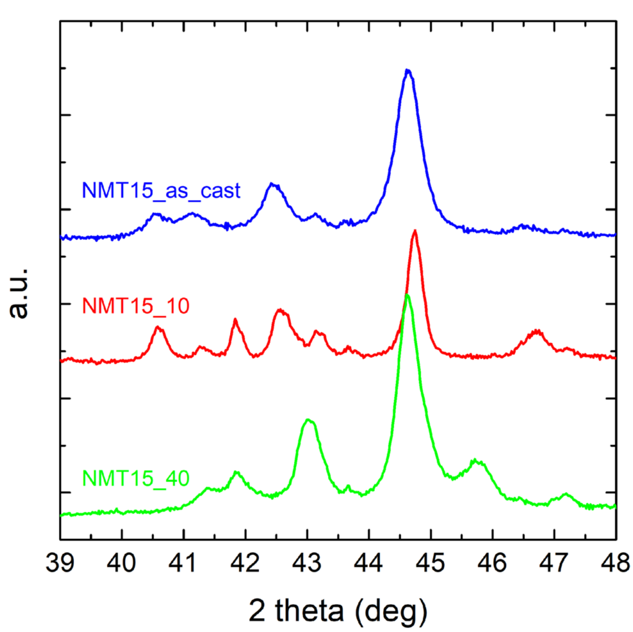

Figure 4 Comparison of the X-ray diffraction analysis of NMT15_10, NMT15_40 produced by melt spinning, and NMT15_as_cast produced by arc melting.

and high (40 m/s) wheel speeds with those in arc-melted (as-cast) samples, offering additional insights. The XRD pattern of the ribbon produced at 10 m/s closely matches that of the as-cast sample obtained via arc melting. In contrast, ribbons produced at higher wheel speeds exhibit a noticeable peak shift toward lower diffraction angles, for instance, the peak at 46.7°, indicating possible changes in lattice parameters or internal stress states. Table 1 summarizes the unit cell parameters derived by Lebail fitting for the monoclinic martensitic phase in the ribbons produced at 40 m/s wheel speed and for the arc-melted sample of the same composition.

Notably, the lattice parameter b of the NMT15_40 ribbon is larger than that of the arc-melted as-cast NMT15 martensite, with a strain of $\Delta b/b = 0.004$, indicating a tensile distortion of the unit cell along b-axis. This effect is consistent with the rapid cooling and highly directional solidification inherent to the melt spinning process [41] and, as previously discussed, suggests the formation of a coherent microstructure

Table 1 Unit cell parameters for martensite phase in NMT15 melt-spun ribbon produced with wheel speed equal to 40 m/s and in arc-melted samples from [17]

Sample	a (Å)	b (Å)	c (Å)	α (°)	β (°)	γ (°)
NMT15 as-cast (arc melting)	4.3325	5.5026	4.2524	90.0	91.04	90.0
NMT15_40 (melt spinning)	4.313	5.527	4.222	90.0	91.03	90.0

compatible with strain defects that broaden the calorimetric response. Additionally, the indexing of the newly observed peaks in samples fabricated at high wheel speed was successfully achieved by introducing a modulation vector $q = 0.40{\cdot}c^*$, where c^* is a reciprocal lattice vector. The significant intensity of the modulation reflection at $2\theta = 45.5°$ suggests pronounced structural distortions induced by the faster cooling rates at wheel speeds exceeding 30 m/s.

Based on the geometrical, microstructural and calorimetric characterizations, NMT15_20 and NMT18_20 samples exhibited the best properties in terms of a favorable balance between sharp martensitic transformation peaks, relatively homogeneous thickness and slightly coarser grains. Therefore, they were selected for further investigation of their mechanical and functional properties.

Mechanical properties and Δ*S* evaluation

The tensile strain recovery tests conducted on NMT15_20 and NMT18_20 samples are shown in Fig. 5. For both alloys, the curves exhibit an inverse strain trend at low applied stresses, where the strain decreases during cooling and increases upon heating. The same trend is observed for all the ribbons, as reported in Figure S1 of *Supplementary Material* for sample NMT15_40. Thus, as observed in the prior calorimetric and microstructural analyses, the mechanical response is consistent with the presence of residual stresses introduced by the rapid solidification process and retained within the material. The influence of solidification rate on the thickness of the ribbons and defect formation is well established in melt-spun systems [30, 42]. In the present work, the variation of wheel speed primarily affects the cooling rate, which likely promotes the formation of structural defects, stored stresses and partially amorphous regions. The mechanical response of ribbons further supports the presence of such defect-related effects at the macroscopic scale. In particular, as already observed in previous works, the presence of such defects and stored stresses in ribbons could induce an inverse strain recovery behavior [28]. By strain recovery measures, it is possible to have an indicative evaluation of the amount of such residual stress, when the inverse behavior resets and the material begins to show usual direct recovery of strain. By linear interpolation of the transformation strain values obtained for each applied stress, it was possible to measure the stress value corresponding to the reset of stored stresses that induce the inverse behavior: For the NMT15_20 sample, this value is 31 MPa, whereas for NMT18_20 it is 22 MPa. The favorable mechanical properties observed in the

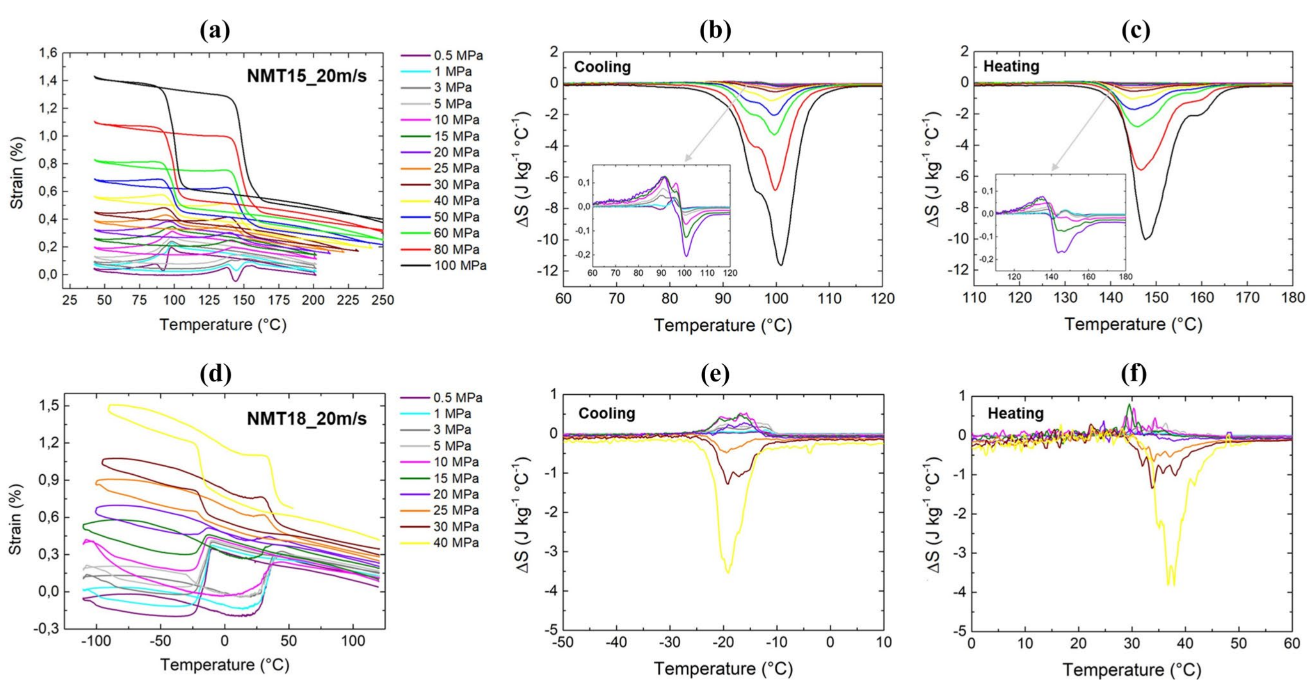

Figure 5 Tensile strain recovery tests for NMT15_20 **a** and NMT18_20 **d** as-spun ribbons. Entropy changes evaluated by means of Maxwell equation during cooling and heating for NMT15_20 **b**, **c** and NMT18_20 **e**, **f** ribbons.

strain recovery tests enhance the interest in developing the elastocaloric performance of these ribbons. No residual strains related to plastic deformation were detected in either alloy. Moreover, NMT15 samples demonstrated superior strength, withstanding constant applied stresses up to 100 MPa before failure, whereas NMT18 samples failed at stresses exceeding 40 MPa. The maximum recoverable tensile load exceeds previously reported values for NiMn-based melt-spun ribbons, such as those based on NiMnGa and NiMnSn [27, 28]. Moreover, the Δ*S* values measured range from 4 J/(kg °C) for NMT18 to 10–12 J/(kg °C) for NMT15, which is a considerable value for NiMn-based melt-spun ribbons [27, 28]. Some preliminary attempts to enhance the strain recovery behavior of NMT18 ribbons by heat treatments are briefly described and discussed in *Supplementary Material*. Specifically, strain recovery and Δ*S* curves are reported in Figure S2 and stress–strain measurements are reported in Figure S3.

Tensile stress–strain tests were performed under isothermal conditions. As expected, in the melt-spun ribbons, the stress–strain behavior is affected by its inherent brittleness and by failure at relatively low tensile strains. Moreover, the tensile loading–unloading curves shown in Figs. 6, 7 exhibit minimal hysteresis and do not show well-defined plateaus, suggesting that the maximum applied stress without failure may be insufficient to induce a complete martensitic transformation. However, even a limited hysteresis is generally associated with the onset of transformation-related processes. In rapidly solidified systems, such as melt-spun ribbons, the mechanical response could be partially influenced by factors such as high defect density, internal stresses and microstructural heterogeneity. Under these conditions, a classical flag-shaped response is not necessarily expected, and transformation-induced features may appear in a more gradual or distributed manner. A similar behavior, including reduced hysteresis and absence of clear plateaus, has been reported in the literature for other NiMn-based systems like sintered NiMnGa [43, 44]. The elastic modulus as a function of temperature shows the highest values, up to 46.5 GPa, for the NMT15 alloy.

Three-point bending tests were carried out under isothermal conditions and low displacement rate, and the main results of as-spun samples are shown in Fig. 8. The experimental setup for three-point bending tests does not involve the fixing of the ribbons in a sample holder, but they lean on the two supports without any deformation constraint. Nevertheless, this experimental condition gives rise to some slipping during the rapid martensite induction and shrinkage in loading and unloading plateau. Due to the inhomogeneous stress distribution inherent to bending and the low fracture strain of the studied ribbons, failure occurred at displacements exceeding 3 mm, corresponding to a maximum strain of 0.6% at the ribbon midpoint, as calculated using Eq. 1:

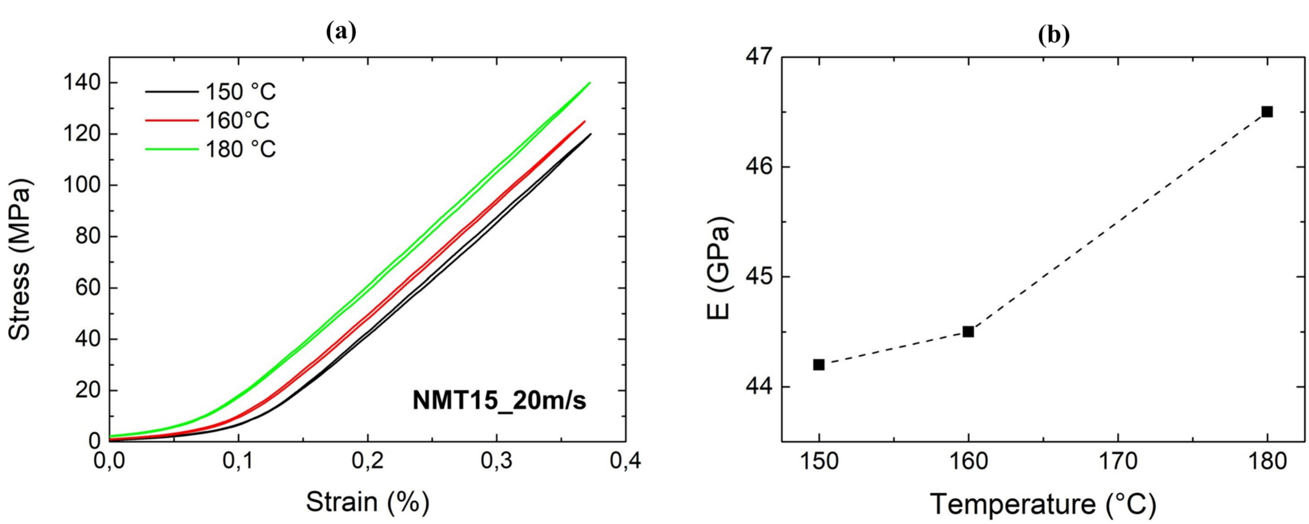

Figure 6 Tensile isothermal mechanical tests starting from Af + 10 °C for NMT15_20 ribbons **a** and trend of the elastic modulus versus temperature **b**.

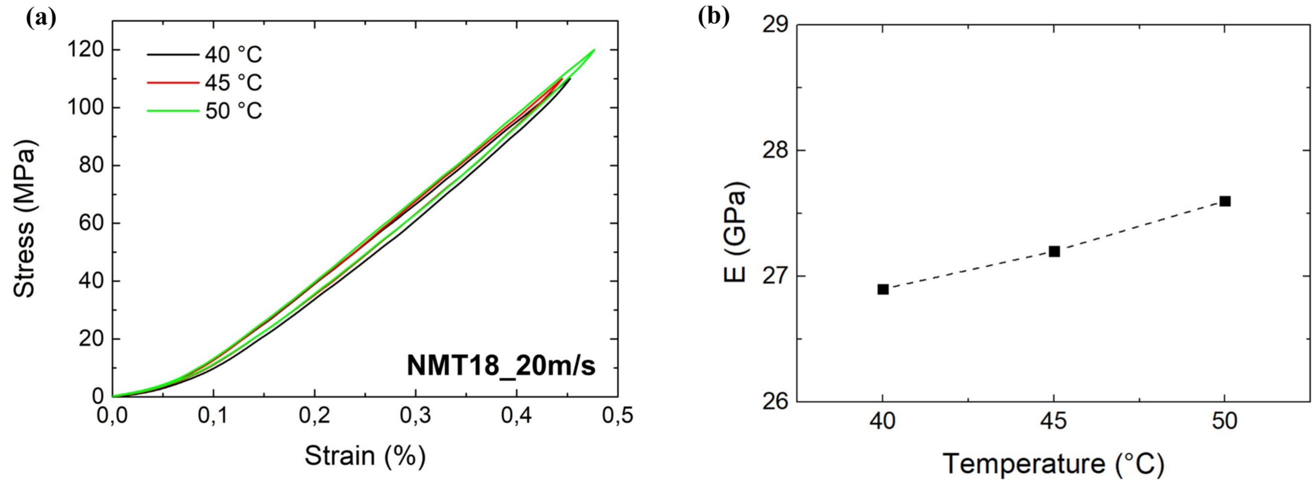

Figure 7 Tensile isothermal mechanical tests starting from Af + 10 °C for NMT18_20 ribbon **a** and trend of the elastic modulus versus temperature **b**.

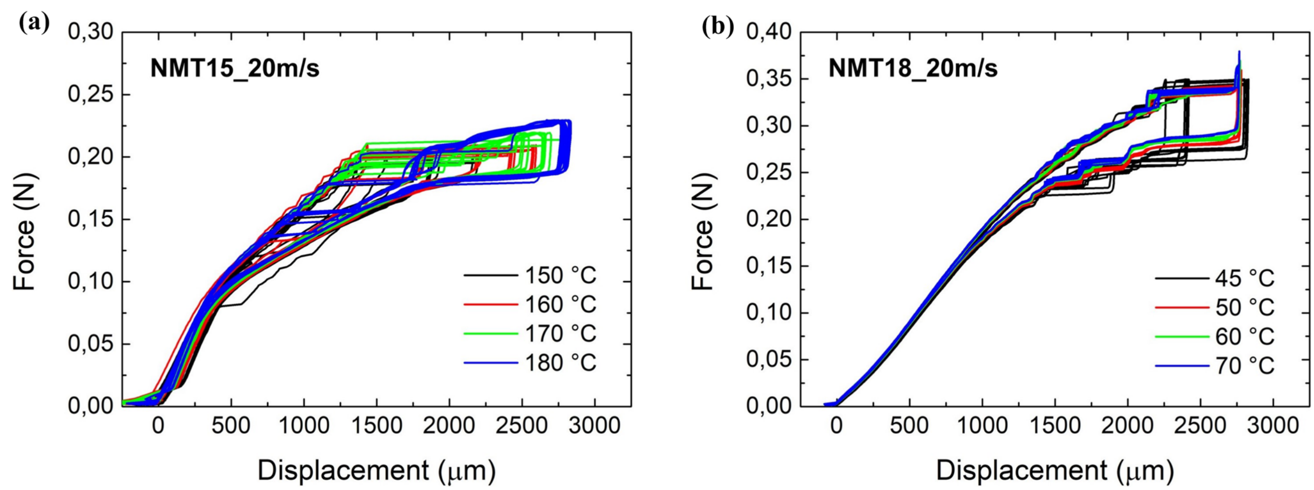

Figure 8 Three-point bending curves performed at different temperatures, starting from Af + 10 °C for NMT15_20 **a** and NMT18_20 **b** as-spun ribbons.

$$\varepsilon = \frac{6Dt}{L^2} \quad (1)$$

where D is the maximum deflection at the midpoint of the sample, t is the sample thickness, and L is the support span, which in the current tests was 10 mm. Martensite induction likely occurs in the material that is able to withstand the applied deformation without failure. However, the recorded mechanical curves, even though they show some steps, indicate the partial induction of martensite, suggesting a potential improvement also in elastocaloric performance under this configuration. Additionally, the mechanical response exhibited good cycling stability to 50 cycles and minimal temperature dependence, as the mechanical cycles conducted at different temperatures yielded similar results.

Despite the limited tensile and bending mechanical properties of NiMnTi ribbons, time-resolved temperature profiles were recorded during quasi-adiabatic unloading in both tensile (Fig. 9a, b) and bending (Fig. 9c, d) configurations. Due to specific experimental constraints, the results are limited by reduced sensitivity in temperature measurement. Indeed, the thermocouple fixture on the ribbon surface inherently limits the achievable temperature change signal. Moreover, the small thickness of the ribbons and their large

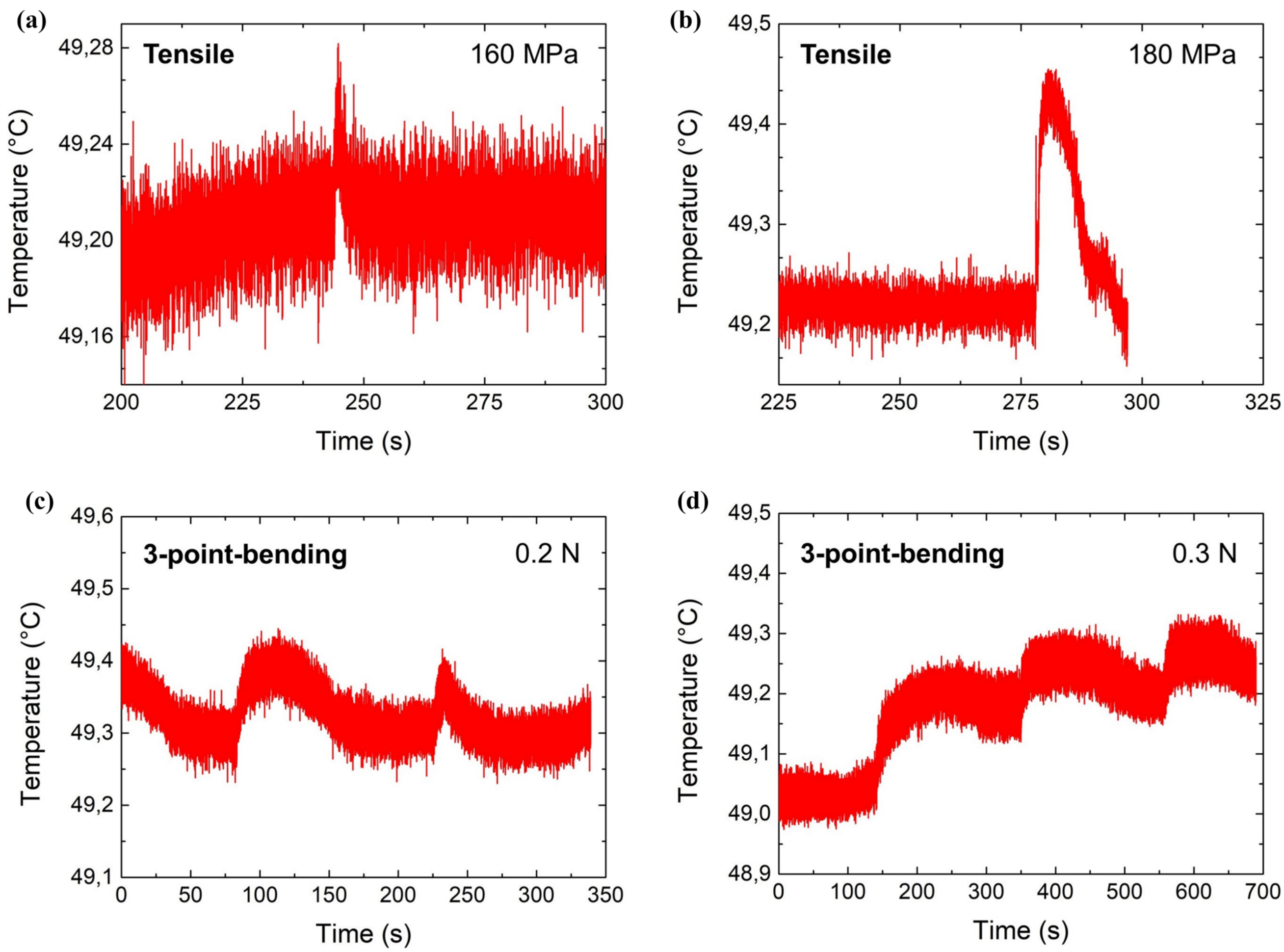

Figure 9 Temperature versus time profiles obtained by quasi-adiabatic unloading of NMT18_20 ribbons in tensile **a**, **b** and three-point bending **c**, **d** configuration.

surface-to-volume ratio enhance heat exchange with the environment, making adiabatic conditions difficult to achieve. As a consequence, the measured temperature changes should be considered as conservative estimates, likely underestimating the actual adiabatic temperature change. Nevertheless, despite the low signal intensity, the detection of small temperature fluctuations in the range of 0.1–0.3 °C during rapid unloading remains noteworthy. This represents an important starting point for improving performance by optimizing ribbon size and heat transfer in devices where flexural deformation is controlled.

Conclusions

Melt spinning is a suitable method for producing NiMnTi ribbons and exploring their potential for various application devices at the microscale. The NiMnTi ribbons produced by melt spinning appear to exhibit characteristic features typical of this processing method, such as strain defects distributed throughout the material and pronounced anisotropic grain growth, both resulting from the rapid solidification process. These features likely affect the thermo-mechanical properties and transformation behavior of ribbons. The produced NiMnTi ribbons exhibit, for the first time, a combination of favorable mechanical properties, absence of plastic deformation, and promising ΔS values (10–12 J/(kg °C)) measured under strain recovery conditions. Among the deformation modes evaluated, bending deformation appears to be the most suitable and promising for the development of applications at the mini—and microscale. In particular, the NMT15 alloy shows superior performance compared to NMT18, especially in temperature ranges above room temperature. These findings suggest that the potential functional properties previously observed in polycrystalline NiMnTi samples may also be retained in melt-spun ribbons. However, the preliminary quasi-adiabatic tests highlight the necessity of further optimization to improve their elastocaloric response.

Acknowledgements

The authors are grateful to Nicola Bennato and Giordano Carcano (CNR ICMATE) for their technical support.

Funding

Open access funding provided by Consiglio Nazionale Delle Ricerche (CNR) within the CRUI-CARE Agreement. Basque Government Department of Education, KK-2024/00048, Daniel Salazar, KK-2025/00034, Daniel Salazar, Spanish Ministry of Science and Innovation, PID2022-138256NA-C22, Daniel Salazar, European Space Agency, 4000148229/2025/NL/GLC, Daniel Salazar.

Data availability

Data will be made available on request.

Declarations

Conflict of interest The authors have no conflict of interests to declare that are relevant to the content of this article.

Supplementary Information The online version contains supplementary material available at https://doi.org/10.1007/s10853-026-13013-2.

References

[1] De Paula VG, Reis MS (2021) All-*d*-metal *full* Heusler alloys: a novel class of functional materials. Chem Mater 33:5483–5495. https://doi.org/10.1021/acs.chemmater.1c01012

[2] Yan H-L, Wang L-D, Liu H-X, Huang X-M, Jia N, Li Z-B, Yang B, Zhang Y-D, Esling C, Zhao X, Zuo L (2019) Giant elastocaloric effect and exceptional mechanical properties in an all-d-metal Ni-Mn-Ti alloy: experimental and ab-initio studies. Mater Des 184:108180. https://doi.org/10.1016/j.matdes.2019.108180

[3] Potapov PL, Polyakova NA, Udovenko VA, Svistunova EL (1996) The martensitic structure and shape memory effect in NiMn alloyed by Ti and Al. Int J Mater Res 87:33–39. https://doi.org/10.1515/ijmr-1996-870105

[4] Guan Z, Bai J, Gu J, Liang X, Liu D, Jiang X, Huang R, Zhang Y, Esling C, Zhao X, Zuo L (2021) First-principles investigation of B2 partial disordered structure, martensitic transformation, elastic and magnetic properties of all-d-metal Ni-Mn-Ti Heusler alloys. J Mater Sci Technol 68:103–111. https://doi.org/10.1016/j.jmst.2020.08.002

[5] Li G, Liu E, Wu G (2022) d-d hybridization controlled large-volume-change martensitic phase transition in Ni-Mn-Ti-based all-d-metal Heusler compounds. J Alloys Compd 923:166369. https://doi.org/10.1016/j.jallcom.2022.166369

[6] Cong D, Xiong W, Planes A, Ren Y, Mañosa L, Cao P, Nie Z, Sun X, Yang Z, Hong X, Wang Y (2019) Colossal elastocaloric effect in ferroelastic Ni-Mn-Ti alloys. Phys Rev Lett 122:255703. https://doi.org/10.1103/PhysRevLett.122.255703

[7] Wei ZY, Sun W, Shen Q, Shen Y, Zhang YF, Liu EK, Liu J (2019) Elastocaloric effect of all-*d*-metal Heusler NiMnTi(Co) magnetic shape memory alloys by digital image correlation and infrared thermography. Appl Phys Lett 114:101903. https://doi.org/10.1063/1.5077076

[8] Yang Z, Cong DY, Sun XM, Nie ZH, Wang YD (2017) Enhanced cyclability of elastocaloric effect in boron-microalloyed Ni-Mn-In magnetic shape memory alloys. Acta Mater 127:33–42. https://doi.org/10.1016/j.actamat.2017.01.025

[9] Yang Z, Cong D, Yuan Y, Wu Y, Nie Z, Li R, Wang Y (2019) Ultrahigh cyclability of a large elastocaloric effect in multiferroic phase-transforming materials. Mater Res Lett 7:137–144. https://doi.org/10.1080/21663831.2019.1566182

[10] Zhang G, Wang H, Li Z, Yang B, Yan H, Zhao X, Zuo L (2023) Colossal elastocaloric effect in a <001>A oriented Ni49Mn33Ti18 polycrystalline alloy. Scr Mater 234:115584. https://doi.org/10.1016/j.scriptamat.2023.115584

[11] Villa F, Villa E, Passaretti F, López-Cruz M, Sánchez Llamazares JL (2025) Investigation of the multicaloric properties in spark plasma sintered NiMnCoTi alloys. J Mater Res Technol 36:9342–9348. https://doi.org/10.1016/j.jmrt.2025.05.187

[12] Wei ZY, Liu EK, Chen JH, Li Y, Liu GD, Luo HZ, Xi XK, Zhang HW, Wang WH, Wu GH (2015) Realization of multifunctional shape-memory ferromagnets in all-*d*-metal Heusler phases. Appl Phys Lett 107:022406. https://doi.org/10.1063/1.4927058

[13] Wei ZY, Liu EK, Li Y, Han XL, Du ZW, Luo HZ, Liu GD, Xi XK, Zhang HW, Wang WH, Wu GH (2016) Magnetostructural martensitic transformations with large volume changes and magneto-strains in all-*d*-metal Heusler alloys. Appl Phys Lett 109:071904. https://doi.org/10.1063/1.4961382

[14] Li B, Liu Z, Li D, Feng Z, Zhu J, Zhong H, Li S (2024) Large reversible multicaloric effects over a broad refrigeration temperature range in Co and B co-doped Ni-Mn-Ti alloys. Mater Sci Eng A 896:146260. https://doi.org/10.1016/j.msea.2024.146260

[15] Sun S, Bai J, Gu J, Guo K, Morley N, Gao Q, Zhang Y, Esling C, Zhao X, Zuo L (2024) Extraordinary mechanical properties and room-temperature magnetocaloric effects in spark plasma sintered all-d-metal Ni-Co-Mn-Ti alloy. J Alloys Compd 976:173406. https://doi.org/10.1016/j.jallcom.2023.173406

[16] Bachagha T, Jing C, Ren W (2024) Magnetocaloric effect and phase transformation of Zn-doped Ni-Mn-Ti all-d metal Heusler alloys. J Alloys Compd 1004:175632. https://doi.org/10.1016/j.jallcom.2024.175632

[17] Villa F, Villa E, Righi L, Ruggieri P, Bennato N, Battiston S, Passaretti F, Casati R (2024) Effect of the thermal processing on the microstructural, functional and mechanical properties of cast polycrystalline NiMnTi alloys. J Alloys Compd 1000:175099. https://doi.org/10.1016/j.jallcom.2024.175099

[18] Villa F, Villa E, Bennato N, Passaretti F, Casati R (2025) Direct and indirect assessment of the elastocaloric properties of cast NiMnTi alloys. J Alloys Compd 1010:177570. https://doi.org/10.1016/j.jallcom.2024.177570

[19] Guan Z, Bai J, Zhang Y, Gu J, Zhang Y, Esling C, Zhao X, Zuo L (2023) Ultrahigh cyclic stability and giant elastocaloric effect in directionally solidified (Ni50Mn28Fe2.5Ti19.5)99.4B0.6 alloy. Scripta Mater 229:115353. https://doi.org/10.1016/j.scriptamat.2023.115353

[20] Zhang G, Wang H, Li Z, Yang B, Yan H, Zuo L (2023) Giant elastocaloric effect covering a wide temperature region in a directionally solidified Ni50Mn30Ti20 alloy. Scr Mater 237:115725. https://doi.org/10.1016/j.scriptamat.2023.115725

[21] Li B, Li S, Yang B, Zhong H, Liu Z, Li D (2023) Enhancing the elastocaloric effect and thermal cycling stability in dendritic-like Ni50Mn31.6Ti18.4 single crystal. J Alloys Compd 936:168310. https://doi.org/10.1016/j.jallcom.2022.168310

[22] Liu K, Ma S, Ma C, Han X, Yu K, Yang S, Zhang Z, Song Y, Luo X, Chen C, Rehman SU, Zhong Z (2019) Martensitic transformation and giant magneto-functional properties in all-d-metal Ni-Co-Mn-Ti alloy ribbons. J Alloys Compd 790:78–92. https://doi.org/10.1016/j.jallcom.2019.03.173

[23] López-Cruz M, Zamora J, Sánchez-Valdés CF, Sánchez Llamazares JL (2021) On the synthesis, structural transformation and magnetocaloric behavior of Ni37.5Co12.5Mn35Ti15 melt-spun ribbons. AIP Adv 11:015010. https://doi.org/10.1063/9.0000163

[24] Ma C, Liu K, Han X, Yang S, Ye N, Tang J (2020) Martensitic transformation and magnetocaloric effect in melt-spun Mn50Ni31.5Co8.5Ti10 all-3d-metal alloy ribbons. J Magn Magn Mater 493:165733. https://doi.org/10.1016/j.jmmm.2019.165733

[25] Neves Bez H, Pathak AK, Biswas A, Zarkevich N, Balema V, Mudryk Y, Johnson DD, Pecharsky VK (2019) Giant enhancement of the magnetocaloric response in Ni-Co-Mn-Ti by rapid solidification. Acta Mater 173:225–230. https://doi.org/10.1016/j.actamat.2019.05.004

[26] Zhang Y, Zeng H, Yu G, Liu K, Ma S, Yang K, Zhao X, Yuan G, Luo X, Chen C, Zhong Z (2020) Impact of annealing on the martensitic transformation and magnetocaloric properties in all-3d-metal Mn50Ni32Co8Ti10 alloy ribbons. Intermetallics 125:106882. https://doi.org/10.1016/j.intermet.2020.106882

[27] Villa E, Aguilar-Ortiz CO, Nespoli A, Álvarez-Alonso P, Camarillo-Garcia JP, Salazar D, Passaretti F, Flores-Zúñiga

H, Hosoda H, Chernenko VA (2019) Tailoring thermomechanical treatment of Ni-Fe-Ga melt-spun ribbons for elastocaloric applications. J Mater Res Technol 8:4540–4546. https://doi.org/10.1016/j.jmrt.2019.07.067

[28] Villa E, Villa F, Crespo BR, Lazpita P, Salazar D, Hosoda H, Chernenko V (2023) Shape memory and elastocaloric properties of melt-spun NiMn-based Heusler alloys. J Alloys Compd 965:171437. https://doi.org/10.1016/j.jallcom.2023.171437

[29] Pons J, Cesari E, Santamarta R, Chernenko VA. (2000) Mechanical properties of NiMnGa and NiTi-based melt-spun ribbons. In: Adv. Mech. Behav. Plast. DAMAGE VOLS 1 2 Proc., France: p. 879–84

[30] Aguilar-Ortiz CO, Camarillo-García JP, Vergara J, Álvarez-Alonso P, Salazar D, Chernenko VA, Flores-Zúñiga H (2018) Effect of solidification rate on martensitic transformation behavior and adiabatic magnetocaloric effect of Ni50Mn35In15 ribbons. J Alloys Compd 748:464–472. https://doi.org/10.1016/j.jallcom.2018.03.074

[31] Norouzi-Inallu M, Ghotbi Varzaneh A, Kameli P, Ullakko K, Chernenko V, Hosoda H, Salazar D. (2023) Transformation Behavior and Inverse Magnetocaloric Effect in $Ni_{45}Co_5Mn_{36.7}In_{13.3-X}Ge_X$ Melt-Spun Ribbons. https://doi.org/10.2139/ssrn.4491292

[32] González-Legarreta L, Caballero-Flores R, Rosa WO, Ipatov M, Escoda L, Suñol JJ, Prida VM, González J, Hernando B. (2016) Heusler alloy ribbons: structure, martensitic transformation, magnetic transitions, and exchange bias effect. In: Zhukov A, editor. Nov. Funct. Magn. Mater., vol. 231, Cham: Springer International Publishing, p. 83–114. https://doi.org/10.1007/978-3-319-26106-5_3

[33] Salazar-Jaramillo D, Barandiaran JM, Kohl M, Cong D, Hosoda H, Sanchez Llamazares JL, Chernenko VA. (2021) Lightweight, multifunctional materials based on magnetic shape memory alloys. Adv. Lightweight Multifunct. Mater., Elsevier, p. 187–237. https://doi.org/10.1016/B978-0-12-818501-8.00005-6

[34] Hernando B, Llamazares JLS, Santos JD, Sánchez ML, Escoda L, Suñol JJ, Varga R, García C, González J (2009) Grain oriented NiMnSn and NiMnIn Heusler alloys ribbons produced by melt spinning: martensitic transformation and magnetic properties. J Magn Magn Mater 321:763–768. https://doi.org/10.1016/j.jmmm.2008.11.105

[35] Yan H, Sánchez-Valdés CF, Zhang Y, Sánchez Llamazares JL, Li Z, Yang B, Esling C, Zhao X, Zuo L (2018) Correlation between crystallographic and microstructural features and low hysteresis behavior in Ni50.0Mn35.25In14.75 melt-spun ribbons. J Alloys Compd 767:544–551. https://doi.org/10.1016/j.jallcom.2018.07.063

[36] Louidi S, Sunol JJ, Ipatov M, Hernando B (2018) Effect of cobalt doping on martensitic transformations and the magnetic properties of Ni50−xCoxMn37Sn13 (x = 1, 2, 3) Heusler ribbons. J Alloys Compd 739:305–310. https://doi.org/10.1016/j.jallcom.2017.12.280

[37] Feng Y, Fang C, Ai Y-L, Wang H-B, Gao L, Chen H, Bian X-H (2023) Crystal orientation in Ni–Mn–In melt-spun ribbons. Rare Met 42:1398–1402. https://doi.org/10.1007/s12598-018-1026-x

[38] Huang S, Qin L, Li Y, Li L (2021) The study of martensitic transformation and magnetocaloric effect in rare earth Y-doped all-d-metal Ni-Co-Mn-Ti Heusler alloys. Mater Lett 302:130376. https://doi.org/10.1016/j.matlet.2021.130376

[39] López-Cruz M, Varga R, Sánchez Llamazares JL (2024) Magnetostructural transformation and magnetocaloric properties of (Ni37.5Co12.5Mn35Ti15)100−xBx (x = 0.0 and 0.4) melt-spun ribbons. Metals Basel 14:216. https://doi.org/10.3390/met14020216

[40] Zhao X, Yan Y, Wen J, Li Y, Li L (2022) Enhancement of magnetocaloric effect in all-d-metal Heusler Mn52.6Ni30.5Co7.8Ti9.1/PVA/PET flexible composite by mechanical strains. J Alloys Compd 897:163116. https://doi.org/10.1016/j.jallcom.2021.163116

[41] Dadda K, Alleg S, Souilah S, Daza J, Saurina J, Suñol J-J, Bessais L, Hlil E-K (2022) Microstructure, critical behavior and magnetocaloric properties of melt-spun Ni51.82Mn32.37In15.81. Magnetochemistry 8:179. https://doi.org/10.3390/magnetochemistry8120179

[42] Álvarez-Alonso P, Aguilar-Ortiz CO, Villa E, Nespoli A, Flores-Zúñiga H, Chernenko VA (2017) Conventional and inverse elastocaloric effect in Ni-Fe-Ga and Ni-Mn-Sn ribbons. Scr Mater 128:36–40. https://doi.org/10.1016/j.scriptamat.2016.09.033

[43] Villa F, Tamandi M, Passaretti F, Bassani E, Villa E (2023) Promising elastocaloric properties of sintered polycrystalline NiMnGa produced by open die pressing. J Mater Sci 58:15240–15250. https://doi.org/10.1007/s10853-023-08977-4

[44] Villa F, Villa E, Bassani E, Tomasi C, Passaretti F, Casati R (2024) A novel sintering method for polycrystalline NiMnGa production for elastocaloric applications. J Mater Res Technol 30:5582–5589. https://doi.org/10.1016/j.jmrt.2024.04.259